ISSN 1028-334X, Doklady Earth Sciences, 2015, Vol. 464, Part 2, pp. 1044–1048. © Pleiades Publishing, Ltd., 2015.
Original Russian Text © K.Zh. Seminsky, R.M. Zaripov, V.V. Olenchenko, 2015, published in Doklady Akademii Nauk, 2015, Vol. 464, No. 4, pp. 480–484.

GEOPHYSICS

Interpretation of the Electrical Resistivity Tomography Data Obtained for Shallow Fault Zones: A Tectonophysical Approach

K. Zh. Seminsky[a], R. M. Zaripov[a], and V. V. Olenchenko[b]

Presented by Academician M.I. Epov June 18, 2014

Received July 8, 2014

Abstract—A new tectonophysical approach to the interpretation of the electrical resistivity tomography of shallow fault zones is proposed. The approach is based on ideas about their stage-to-stage development, which suggests a regular occurrence of different designation levels of the rock substratum. The levels distinguished on the basis of a statistical analysis of ERT data allow one to determine the boundaries of the fault zone and inner subzones, connected with the formation of the main fault plane and second-order fractures, on a geoelectrical section.

Keywords: fault zone, electrical resistivity tomography.

DOI: 10.1134/S1028334X15100098

The method of shallow electrical resistivity tomography (ERT), an updated variant of the vertical electrical sounding method, has recently been used widely for studying active fault zones in the Earth's crust within poorly exposed areas [1–4], etc. The ERT method allows one to make geoelectric sections of the rock mass. The geological interpretation of sections is based on correlation of beds homogenous in geoelectrical resistivity (ER) with specific types of rocks. Here, fault zones are related to gradient zones of the section or in the central part of linearized zones with low resistivity. The approach proposed for interpretation of massifs with a complex dislocation structure without using a priori information and/or integration with other geophysical methods yields mixed results. In particular, this is due to the fact that faults are regarded as unevenly dislocated geological bodies, which is a reason for the complex spatial ER distribution in rocks (ρ).

According to the tectonophysical patterns, fault zones contain joints and fractures of various ranks, which are related genetically to the development of the main fault plane. Along with the initial stages of elastic plastic deformations, the complete cycle of fault development includes three successive disjunctive stages of formation of shear zones [5, 6]. At the early disjunctive stage, a wide zone of relatively minor fissures forms. In the geological literature, this zone is called a zone of excessive jointing, a blind fault zone, etc. At the late disjunctive stage, a fault zone is represented by an essentially smaller zone of distribution of active fractures (small fragments of the main fault plane, separated nondeformed zones). At the stage of complete destruction, a fault zone is the main fault plane conjugated with large feather faults made of "loose" tectonites (clay gouge, crush breccia, etc.). As a sequence, fault zones in tectonically active regions have a transversely zonal structure due to superimposition of structures from different stages. Here, subzones corresponding to the stage of complete destruction (I) and early (II) and late (II) disjunctive stages, change successively from the axis to the limbs. This zonal sequence is regularly manifested in the designation level of the rock mass and, accordingly, in the field of ER data distribution.

Our study is aimed to develop the principles of a tectonophysical approach to the interpretation of the electrical tomography data obtained during studying shallow active fault zones in southeastern Siberia. The targets of our research, more than 30 active fault zones, are confined to the Baikal rift and adjacent, less active, regions of the Peri-Baikal and Trans-Baikal regions. Most of the steeply dipping different-rank fault zones are confined to the rift shoulders in the Olkhon Island area, in western Peri-Baikal.

In order to perform electrical tomography and to obtain the most complete information about the structure of a fault zone, loose sediment-free sites were

[a] *Institute of the Earth's Crust, Siberian Branch, Russian Academy of Sciences, ul. Lermontova 128, Irkutsk, 664033 Russia*

[b] *Institute of Petroleum Geology and Geophysics, Siberian Branch, Russian Academy of Sciences, pr. Akademika Koptyuga 3, Novosibirsk, 630090 Russia*

e-mail: seminsky@crust.irk.ru, rassell88@yandex.ru, OlenchenkoVV@ipgg.sbras.ru

chosen. In most cases, the fracture density per meter or per square meter was measured, and the geostructural and some other features of fault planes and the rock mass were studied. Sometimes, the relief of a scarp made it possible to determine the position of the main fault plane above which the ERT profile is conducted.

For electrical tomography the geoelectric multielectrode station SCALA 48 was used [7]. The method of determination of geoelectrical resistivity was tested at different sites in the Olkhon Island area, western Peri-Baikal [9]. Measurements were carried out on a Schlumberger array with the distance between electrodes ranging from 1 to 5 m.

Resistivity data were then inverted with Res2DInv [8]. The geostructural data and the data obtained from geoelectric section no. 61, extending for a distance of about 28 km, were used as source data for our interpretation.

According to the geostructural data available, fault zones crossing ancient metamorphic complexes in the Olkhon area are distinguished on the basis of the mapping of zones of higher concentrations of fractures and fault zones. The statistical analysis of the distribution of the fracture density parameter D allowed us to reveal five levels (I–V in Fig. 1a). All levels show similar fracture frequency characteristics. Level III is characterized by the maximum frequency of occurrence; other levels form symmetrical pairs on each of the descending arms of the normal D distribution, as a whole. Here, sparse rock blocks (level V), situated in the geodynamically active Olkhon area are represented by small solid blocks (aplitic granites, migmatite sublayers, etc.) with a sparse network of visible fractures. It was established that uplifted (more stable) sites within the Olkhon area (on the regional scale) are characterized by nearly the same boundary values $D = 6$, 10, 16, and 24 fractures per square meter (Fig. 1a). For lower (less stable) sites the analogous boundary values are somewhat less.

Besides the fracture density distribution, five levels (I–V) of the ER distribution were distinguished within fault zones in the Olkhon area (Fig. 1b). Similar results obtained for fault zones of the Peri-Baikal and Trans-Baikal regions were similar in a qualitative sense (five levels), but different in a quantitative sense (boundary values). Spatially, sites with a higher fracture density in bedrocks correspond to those with lower ER values. This regularity is shown for the example of a fault zone on Cape Ontkhoi (Olkhon area) (Fig. 2) as histograms of the D and ρ distributions (Fig. 1).

Cape Ontkhoi is made of granites and gneissogranites, faulted by a Precambrian mylonite zone. The stress concentration beyond the Precambrian led to the formation of a brittle fault zone made of intensively fractured and weathered rocks. This zone is comprised of the main fault plane and a few secondary fault planes (zones of strongly fractured rocks). Geoelectrical resistivity profiles were conducted (Fig. 2b),

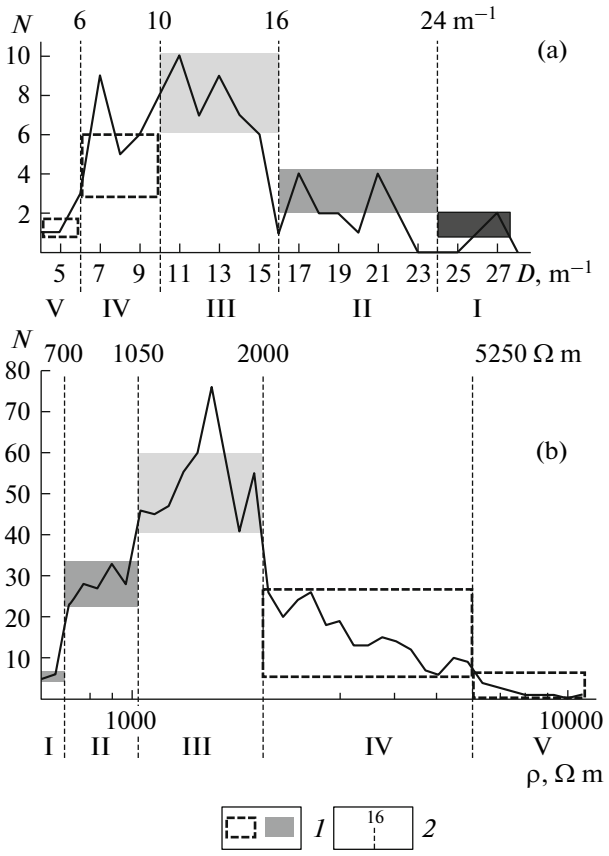

Fig. 1. Histograms of fracture density D (a) and the ER data ρ (b) distributions in a fault zone on Cape Ontkhoi, Western Peri-Baikal: *1*, sections of histograms with series of D or ρ values, similar in frequency of occurrence; *2*, boundaries of sites corresponding to five (I–V) designation levels of the rock mass, which are regularly different in boundary parameters D and ρ due to stage-to-stage formation of the fault zone.

and geostructural measurements including study of the fracture density distribution (Fig. 2a) were performed across the strike of the zone.

Analysis of the structural data shows (Fig. 2a) that one of the fault planes is associated with the first designation level (I), and other fault planes are associated with the second level (II), which discontinuously spread along the geoelectrical profile. Level III is also characterized by discontinuous distribution and correlated with sites of the massif with a dense network of fractures. Some large fractures show small displacements and sliding surfaces. Sites with a low designation level (<10 fractures per meter) are located in marginal parts of the profile. In order to reveal the main regularity in the structure of the fault zone, the designation level of its substratum (Fig. 2a) was generalized based on an uniform approach to analysis of the distribution of each of the boundary D values (10, 16, and 24 fractures per meter). For example, along with sites with $D \geq 16$ and $D \geq 10$ fractures per meter, small intermediate sections of a profile with $D \geq 16$ and $D \geq 10$ frac-

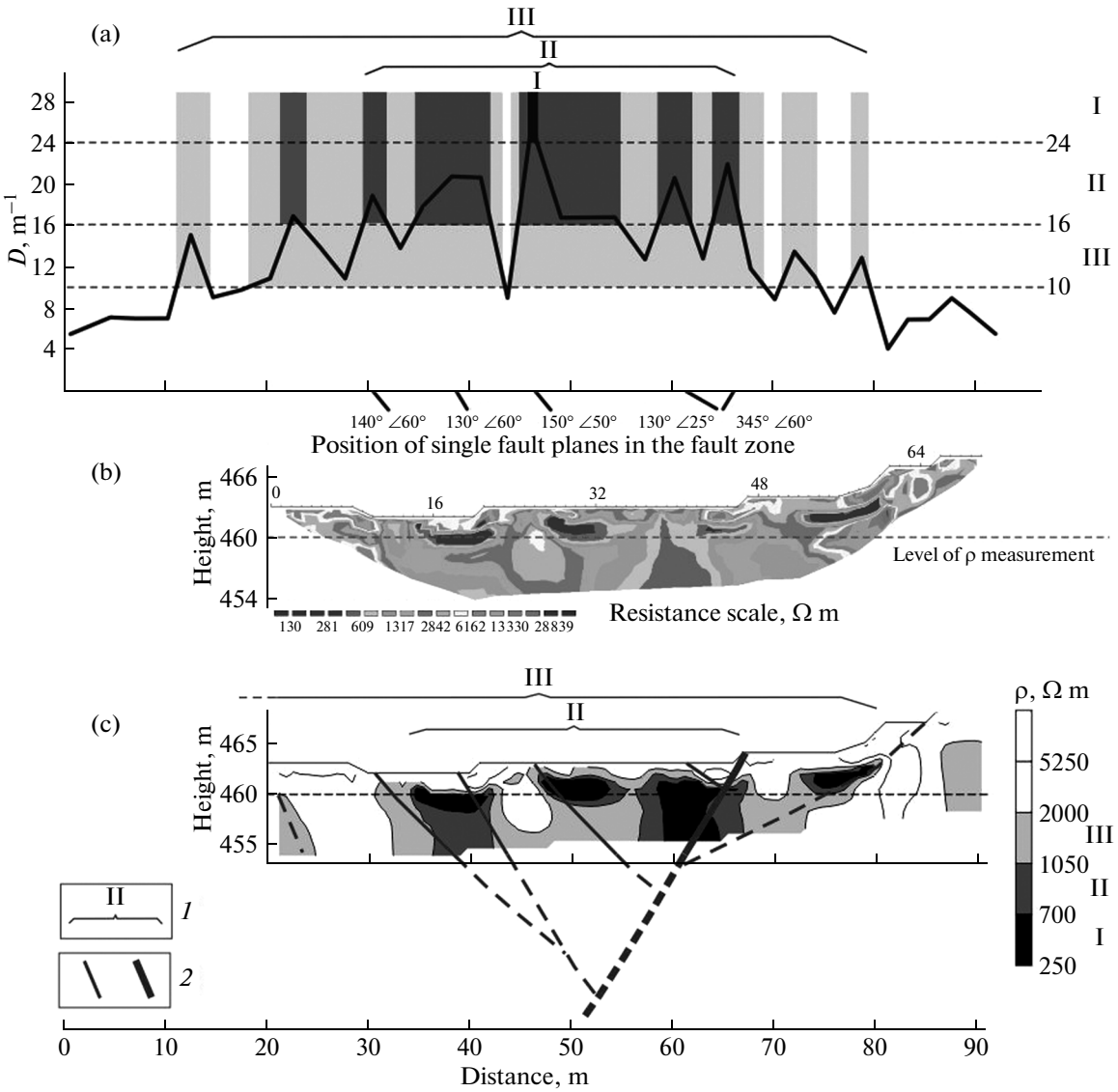

Fig. 2. Results of using a tectonophysical approach for interpretation of the geostructural and ET data from the geoelectrical profile across the fault zone on Cape Ontkhoi (Olkhon area, West Peri-Baikal). (a) Fracture density variations per meter (D). Sites where the rock designation level exceeds three boundary levels D determined by the statistical method (dashed contour) are shown in gray in the diagram. In the lower part are the positions and strike and dip of fault planes of the fault zone. (b)–(c) Geoelectrical sections, constructed based on the ER data, measured along the profile conducted along the coastal cliff of Cape Ontkhoi: (b) standard isolines, (c) ρ isolines determined from statistical analysis of the data set obtained (Fig. 1b). *1*, Generalized boundaries of the fault zone (III) and subzones, which are characterized by a similar level of the rock substratum designation (II, I), according to the results of statistical analysis of distributions D and ρ; *2*, secondary and main fault planes (the proposed position is shown dashed).

tures per meter were referred to levels II and III, respectively. This decision was based on the fact that their dimensions were less than one or both adjacent sections of a profile with $D \geq 16$ and $D \geq 10$ fractures per meter for levels II and III, respectively. The result of generalization, shown in square brackets in the upper part of Fig. 2a, characterizes the transversal zoning of the fault zone that experienced all three (I–III) stages of development.

The geoelectrical section across the fault zone on Cape Ontkhoi (Fig. 2b) is characterized by a wide range of ER values, from a few hundred to a few tens of thousands Ω m, due to the varying designation level of the rock substratum and the varying rock moisture. The uppermost part of the section (1.5–2 m) is an aeration zone with corresponding higher to high ρ values (2000—10 000 Ω m), which was under slightly wet conditions in the survey period. The ER values measured in the lower part of the section, determined by the volume of moisture of the rock mass as a whole, decreases regularly with increasing fracture density in sites corresponding to early (III), late (II), and terminal (I) stages of development of the fault zone.

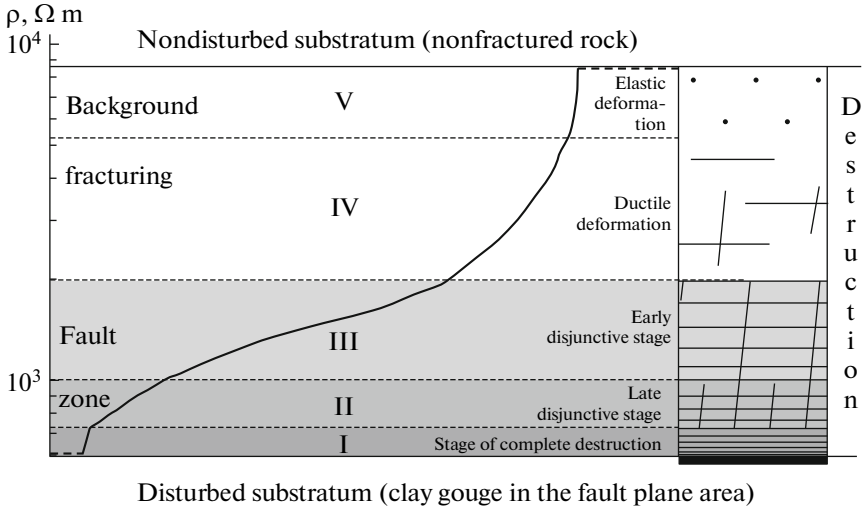

Fig. 3. Generalized diagram of ρ distribution in increasing order, illustrating five (I–V) designation levels of the rock mass (a simplified view of fracture nets is shown on the right) within the near-surface area of the Earth's crust with a fault zone that has experienced all stages of development. The ρ distribution plot is constructed based on the data in Fig. 1b.

The zonal structure of the fault zone is illustrated in Fig. 2c, where ρ isolines are boundary values for levels I–III. Near the surface this pattern of the ER data distribution corresponds to the mapped structure of the fault zone (Fig. 2a) as far as it is possible under conditions when the effect of uneven moisture along with the designation level of the rock mass influence the ρ value. It is important that the generalized boundaries of the largest subzones, II and III by volume, coincide. As for subzone I, then, besides the site revealed on the basis of the *D* parameter distribution, three other sites with a similar designation level of the rock substratum are distinguished on the geoelecrical profile. They are spatially correlated with other fractures, which determine the specific profile of the fault zone structure (Fig. 2c). Here, if we compare sites according to their dimensions, the fault plane with a strike and dip of 345° and ∠ 60° should be considered to be the main one. Thus, the survey results at the Ontkhoi test site show the advantages of the ERT method and a new approach to the interpretation of the results obtained, which allow one to obtain very informative data about the structure of shallow fault zones.

The satisfactory similarity of the transversal zonal patterns of fault zones, revealed with a unified approach to analysis of the ET and geostructural data, as well as the connection of these data with the stages of faulting, allow one to illustrate the electrical resistivity (ER) variations in the disturbed rock mass as a generalized diagram (Fig. 3). The curve on this diagram was constructed based on the same dataset as the ET data distribution in Fig. 1b. However, this curve allows one to illustrate in detail the stages of deformation of the rock mass. The curve was created based on generalization of the measured ρ values arranged in ascending order. The upper and lower sections of the curve, shown dashed as they were fixed on unit profiles, are levels separating actually nondisturbed (a rock mass with ρ of ten and hundreds of thousands Ω m) and completely destroyed rock substrates (clay gouge in a fault plane with ρ = 3–30 Ω m) from the main field of the diagram reflecting different stages of deformation.

The ER values at sites V and IV are regarded as background values reflecting elastic and ductile deformations, respectively. These fields are characterized by a significant decrease (up to a few thousand Ω m) in the ER values in the case of appearance of microfractures (V) and macrofractures (IV) in the bedrock. It is likely that a sparse network of these fractures can include nontectonic fractures (planetary jointing, etc.). According to the tectonophysical approach, the ER values measured at site III correspond to the fault zone, since they reflect the designation level of the rock mass at an early stage of development. Such a designation level of rocks in geodynamically active regions is most common due to superimposition of different-age stages of deformation (the flattened section of the curve). This fact, as well as the absence of large fault planes at sites of the respective type, is a reason why geologists refer them to background values. The ρ values corresponding to site II are less common in the rock mass, since they indicate the designation level of rocks at a late stage of development (strain localization). This is manifested by an increase in the fracture density and the development of large fault planes represented by loose tectonites. The low ER values at site I are stipulated by the rock substratum, represented by low-resistance crushed rock material formed as a result of movements along large feather fractures and the main fault plane at the stage of complete destruction.

The diagram (Fig. 3) is a theoretical basis for tectonophysical interpretation of the ERT data in geodynamically active regions. The practical realization of this tectonophysical approach has been formalized to an adequate degree, and it includes construction of a histogram of the ρ distribution and the subsequent analysis (Fig. 1b). Then, selection of five levels of the rock substratum designation, as well as determination of the corresponding sites of the rock mass on the geoelectrical massif, follows (Fig. 2c). Next, the generalization of the diagram made it possible to distinguish the boundaries of the fault zone and the most deformed fragments formed at the late and terminal stages of the faulting. This approach allows one to determine the quantitative relations between parameters ρ and *D* for every level. Accordingly, this makes it possible to improve the effectiveness of this approach for solution of applied problems. For this purpose, experience of investigations in different types of environments, where these parameters are variable and the ρ distribution is complicated by nontectonic factors (the cover of loose sediments and weathering products, ore mineralization, water-saturated, and freezing areas, etc.), is needed.

ACKNOWLEDGMENTS

We are grateful to our colleagues from the Laboratory of Tectonophysics of IEC Siberian Branch, Russian Academy of Sciences, A.V. Cheremnykh, A.A. Bobrov, Yu.P. Burzunova, and A.S. Cheremnykh for their assistance in the collection and processing of the field material, as well as Academician M.I. Epov for valuable advice and remarks made during preparation of the manuscript.

REFERENCES

1. L. Improta, L. Ferranti, P. M. De Martini, S. Piscitelli, P. P. Bruno, P. Burrato, R. Civico, A. Giocoli, M. Iorio, G. D'Addezio, and L. Maschio, J. Geophys. Res. **115**, B11307 (2010). doi:10.1029/2010JB000871
2. Z. N. Kuria, T. Woldai, F. D. Van der Meer, and J. O. Barongo, J. Afr. Earth Sci. **57**, 345–359 (2010).
3. C. Schutze, T. Vienken, U. Werban, P. Dietrich, A. Finizola, C. Leven, J. Appl. Geophys. **82**, 129–136 (2012).
4. D. Carbonel, F. Gutiérrez, R. Linares, C. Roqué, M. Zarroca, J. McCalpin, J. Guerrero, V. Rodríguez, Geomorphol. **189** (1), 93–108 (2013). doi: 10.1016/j.geomorph.2013.01.020
5. K. Zh. Seminsky, *The Inner Structure of Continental Fault Zones: A Tectonophysical Aspect* (Geo, Novosibirsk, 2003) [in Russian].
6. K. Zh. Seminsky and Yu. P. Burzunova, Dokl. Akad. Nauk **404** (4), 514–517 (2005).
7. *Multielectrode Electrical Resistivity and Induced Polarization Station "Skala-48," A Manual* (INGG SO RAN, Novosibirsk, 2010) [in Russian].
8. M. H. Loke, *Tutorial. RES2DINV Ver. 3.59, Rapid 2-D Resistivity and IP Inversion Using the Least-Squares Method* (Geotomo Software, Malaysia, 2010).
9. R. M. Zaripov, in *The Trofimuk Readings-2013* (INGG, Novosibirsk, 2013), pp. 271–274 [in Russian].

Translated by Dm. Voroschuk